Giant Spin-Orbit Splitting in Inverted InAs/GaSb Double Quantum Wells

Fabrizio Nichele,[1,*] Morten Kjaergaard,[1] Henri J. Suominen,[1] Rafal Skolasinski,[2] Michael Wimmer,[2] Binh-Minh Nguyen,[3] Andrey A. Kiselev,[3] Wei Yi,[3] Marko Sokolich,[3] Michael J. Manfra,[4] Fanming Qu,[2] Arjan J. A. Beukman,[2] Leo P. Kouwenhoven,[2] and Charles M. Marcus[1]

[1]*Center for Quantum Devices and Station Q Copenhagen, Niels Bohr Institute, University of Copenhagen, Universitetsparken 5, 2100 Copenhagen, Denmark*

[2]*QuTech, Delft University of Technology, 2600 GA Delft, The Netherlands*

[3]*HRL Laboratories, 3011 Malibu Canyon Road, Malibu, California 90265, USA*

[4]*Department of Physics and Astronomy and Station Q Purdue, Purdue University, West Lafayette, Indiana 47907, USA, School of Materials Engineering, Purdue University, West Lafayette, Indiana 47907, USA, School of Electrical and Computer Engineering, Purdue University, West Lafayette, Indiana 47907, USA. and Birck Nanotechnology Center, Purdue University, West Lafayette, Indiana 47907, USA*

(Received 4 May 2016; revised manuscript received 10 October 2016; published 5 January 2017)

Transport measurements in inverted InAs/GaSb quantum wells reveal a giant spin-orbit splitting of the energy bands close to the hybridization gap. The splitting results from the interplay of electron-hole mixing and spin-orbit coupling, and can exceed the hybridization gap. We experimentally investigate the band splitting as a function of top gate voltage for both electronlike and holelike states. Unlike conventional, noninverted two-dimensional electron gases, the Fermi energy in InAs/GaSb can cross a single spin-resolved band, resulting in full spin-orbit polarization. In the fully polarized regime we observe exotic transport phenomena such as quantum Hall plateaus evolving in e^2/h steps and a nontrivial Berry phase.

DOI: 10.1103/PhysRevLett.118.016801

The InAs/GaSb double quantum well (QW) shows a peculiar band alignment, with the InAs conduction band and the GaSb valence band residing very close in energy. Shifting the bands by tuning the QW thickness or applying a perpendicular electric field yields a rich electronic phase diagram [1–4]. When the InAs conduction band resides higher than the GaSb valence band, the band structure of a trivial insulator is obtained. By lowering the InAs conduction band below the GaSb valence band, a small hybridization gap opens at finite k vectors [1]. Beyond topological-insulator behavior, expected to emerge in the hybridization gap [2,5–9], the impact of the inverted band structure on transport remains largely unexplored.

Here, we investigate experimentally and numerically how the combination of spin-orbit coupling (SOC) and electron-hole mixing results in a giant band splitting in InAs/GaSb heterostructures close to the hybridization gap. The two resulting subbands, with opposite spin-orbit eigenvalue and different carrier densities, contribute to transport in parallel, and can be detected via magnetotransport measurements. These results are of potential value to semiconductor spintronics, where two-dimensional electron gases (2DEGs) with sizable spin-orbit splittings at low density are desirable [10].

To quantify SOC directly from experimental data, without relying on any particular model, we use the spin-orbit polarization $(n_1 - n_2)/(n_1 + n_2)$, with $n_{1,2}$ the carrier densities of the split spin-orbit subbands [11]. In Rashba systems, the larger the SOC parameter α, the larger the density difference of the subbands at the Fermi energy, with α typically increasing with density [12]. However, the spin-orbit polarization is usually smaller than 15%, even for 2DEGs with large SOC such as InAs, InSb, or HgTe [13–18], while values up to 40% are reached in GaAs or HgTe hole gases [19–22]. In contrast, we find that the hybridized band structure of InAs/GaSb results in two striking peculiarities: first, the spin-orbit polarization increases approaching the charge neutrality point (CNP); second, the spin-orbit polarization reaches 100%.

Experiments were performed on a 12.5 nm InAs, 5 nm GaSb structure patterned in a $100 \times 50\ \mu\text{m}^2$ Hall bar geometry oriented along the [110] crystallographic direction and covered with a global top gate. Magnetotransport measurements used conventional low-frequency lock-in techniques at a temperature of 50 mK. Additional information on the wafer structure, sample fabrication, and measurement techniques are provided in the Supplemental Material [23].

To realistically model our device, we first determine the band alignment as a function of top gate voltage V_{TG}, using a parallel plate capacitor model [3] discussed in the Supplemental Material [23]. The model predicts the density dependence for electrons (n) and holes (p) shown in Fig. 1(a). For $V_{\text{TG}} > -0.2$ V, only electrons are present in the system, with the kink in n at $V_{\text{TG}} = -0.2$ V coinciding with the onset of hole accumulation. Once the hole layer is populated, it partially screens the electrons from being further depleted via the top gate. The hybridization gap is expected at the CNP, when $n = p$. The calculated electrostatic potential is then used for a V_{TG}

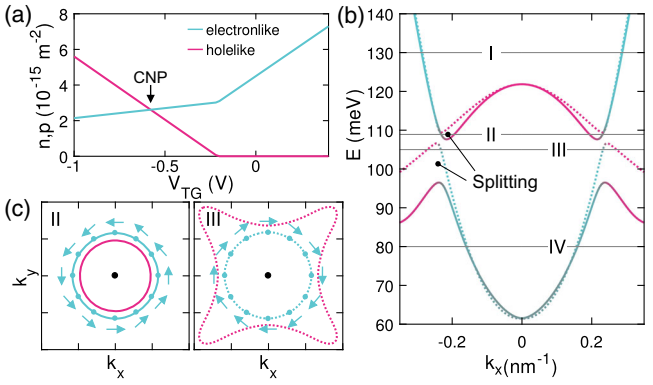

FIG. 1. (a) Expected electron and hole densities dependence on V_{TG}. (b) Numerical band structure calculation for $V_{\mathrm{TG}} = -0.4$ V. The color indicates the wave function main character, solid and dotted lines distinguish two spin-orbit split subbands. (c) Fermi contours and spin texture of electronlike states for the Fermi energies II and III indicated in (b). The axis divisions are 0.2 nm^{-1}, with the black dot indicating the origin. Fermi pockets at large k vector are ignored, but discussed further in the Supplemental Material [23].

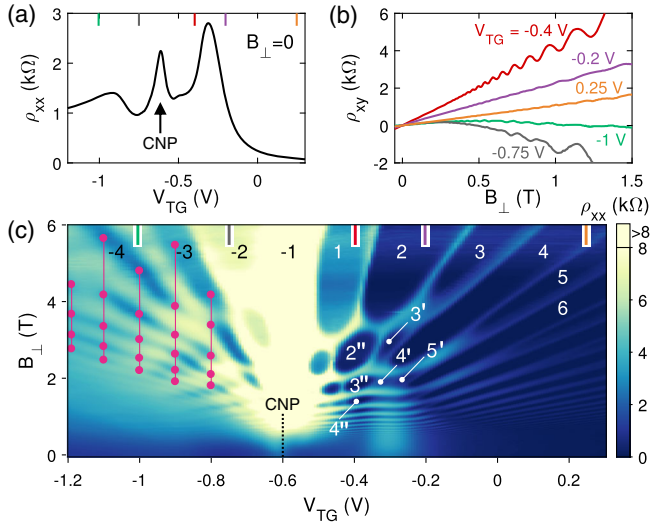

FIG. 2. (a) Longitudinal resistivity ρ_{xx} as a function of top gate voltage for $B_\perp = 0$, with the position of the charge neutrality point indicated. (b) Transverse resistivity ρ_{xy} as a function of $B_\perp$ for different values of V_{TG}, as also indicated by the markers in (a) and (c). (c) ρ_{xx} as a function of V_{TG} and $B_\perp$, with positive (negative) numbering indicating electronlike (holelike) LLs. Pink dots denote holelike filling factors and are used to extract the hole density shown in Fig. 3(c).

dependent band structure simulation using standard $\boldsymbol{k}\cdot\boldsymbol{p}$ theory [23]. In particular, we are interested in the band structure of our system close to the CNP.

The band structure for $V_{\mathrm{TG}} = -0.4$ V is presented in Fig. 1(b). The band coloring represents the calculated wave function character (blue for electronlike and pink for holelike states, also recognizable from the band curvature) while solid and dotted lines distinguish the spin-orbit species. In this configuration, electron and hole bands are inverted and hybridized, with a small gap at finite k vectors. Results for different gate voltages, shown in the Supplemental Material [23], are qualitatively similar but with a varying band overlap. Remarkably, SOC vertically splits the hybridized bands by a sizable amount, resulting in a spin dependent hybridization gap. In this unique band structure, the Fermi energy can cross a *single* branch of the spin-split bands, as indicated by the energy levels II and III in Fig. 1(b). In these situations the system contains both electron- and holelike carriers, and the carriers of the same kind are fully spin-orbit polarized. This effect is prominent close to the bands crossing and negligible far from the hybridization gap [see I and IV in Fig. 1(b)], as expected for individual InAs and GaSb QWs. While the gap size and the bands overlap depend on V_{TG}, the giant splitting at the CNP is a generic feature of the model. Qualitatively similar results were also obtained in previous calculations [2,37–39]. The simulation is consistent with our experiments, where we measure no clear gapped region at the CNP, but a giant spin-orbit splitting of electron- and holelike states.

Fermi contours for energy levels II and III are shown in Fig. 1(c), together with the calculated spin texture of electronlike states. The model indicates Rashba-like spin orientation with spins nearly perpendicular to the momentum direction, with small deviations due to the absence of axial symmetry. This situation is reminiscent of Dirac materials such as graphene or three-dimensional topological insulators, and signatures of Berry phase effects can be expected. Holelike states are instead highly anisotropic.

Magnetotransport measurements, shown in Fig. 2, confirm the sample has an inverted band structure, and is tunable from a pure electron regime to a mixed electron-hole regime. Typical for high mobility structures [3,40], the longitudinal resistivity ρ_{xx} exhibits a series of peaks and dips as a function of V_{TG}, as shown in Fig. 2(a). The resistance peaks at $V_{\mathrm{TG}} = -0.60$ V and $V_{\mathrm{TG}} = -0.35$ V are interpreted with the Fermi energy crossing the CNP and the valence band top, respectively [3], as discussed in reference to Fig. 3(c). In Ref. [40] a resistance dip in the hole-dominated region, similar to what we observe at $V_{\mathrm{TG}} = -0.75$ V, was identified as a van Hove singularity at the bottom of the hybridization gap.

Figure 2(b) shows the transverse resistivity ρ_{xy} as a function of perpendicular field $B_\perp$ for different values of V_{TG}. For $V_{\mathrm{TG}} > -0.4$ V, ρ_{xy} has a positive slope, indicative of exclusively electronlike transport. For $V_{\mathrm{TG}} \leq -0.75$ V, the ρ_{xy} slope reverses at finite $B_\perp$, a hallmark of the simultaneous presence of electrons and holes in the system. This behavior persists down to $V_{\mathrm{TG}} = -1.2$ V, indicating that a pure hole state is not reached in the gate range of operation, consistent with the calculation of Fig. 1(a).

The ambipolar behavior discussed above in terms of ρ_{xy} also becomes apparent in ρ_{xx} in large perpendicular magnetic fields, where Shubnikov–de Haas (SdH)

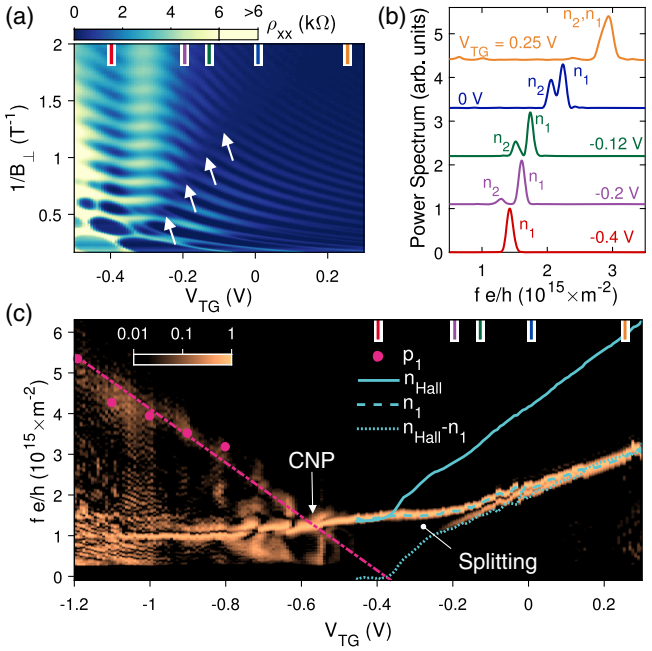

FIG. 3. (a) Longitudinal resistivity ρ_{xx} as in Fig. 2(c) for $V_{TG} \geq -0.5$ V as a function of $1/B_\perp$. The arrows indicate a beating in the SdH oscillations, visible as a π phase shift. (b) Normalized power spectrum of $\rho_{xx}(1/B_\perp)$ for various gate voltages (data offset for clarity). The frequency axis has been multiplied by e/h to directly show the subband densities. (c) Color map of the power spectrum as in (b) as a function of V_{TG}. The amplitude of the power spectrum has been normalized, column by column, to the n_1 peak. The solid blue line indicates the density obtained from the Hall slope, the dashed line marks the n_1 peak, and the dotted line gives the difference between the two. Dots indicate the hole density obtained from holelike LLs in Fig. 2(c), with the dash-dotted line being a guide to the eye.

oscillations and quantum Hall states develop in the entire gate range [Fig. 2(c)]. For $V_{TG} \geq -0.2$ V, we observe regular electronlike Landau levels (LLs) with Zeeman splitting at high field, as indicated by the numbering in Fig. 2(c), obtained from ρ_{xy}. The large resistance increase as a function of $B_\perp$ for $V_{TG} \approx -0.6$ V is consistent with an identical number of electron and hole LLs at the CNP [41,42].

For $V_{TG} \leq -0.5$ V, electronlike and holelike LLs coexist, as also evident from the nonmonotonic ρ_{xy} [see Fig. 2(b)]. In this regime, signatures of electron-hole hybridization are visible as avoided crossings between LLs, as previously observed via cyclotron resonances [43,44]. Based on the analysis presented in Fig. 3(c), we assign to the holelike LLs the filling factors indicated with negative numbering. Approaching the CNP from the electron regime, a peculiar closing and reopening of spin-split levels takes place, as marked with primed numbers. This is associated with the spin-orbit splitting becoming larger than the LL separation. An additional evolution of the LLs takes places for $V_{TG} \approx -0.4$ V, as indicated with double-primed numbering. As discussed in the following, this is associated with the depopulation of one split subband. Filling factors assigned to primed and double-primed LLs are confirmed by ρ_{xy} measurements.

We now address the electronlike states close to the hybridization gap. Low-field SdH oscillations are a powerful tool to study properties at the Fermi surface such as electron density and effective mass [45,46]. In systems where two subbands contribute to transport in parallel, as 2DEGs with strong SOC, the SdH oscillations manifest a beating pattern given by the superposition of two sets of oscillations with different $1/B_\perp$ periodicity [13–18,47]. The power spectrum of $\rho_{xx}(1/B_\perp)$ then allows one to extract the density components n_i from the peak frequencies f_i as $n_i = ef_i/h$ [12]. The SdH analysis gives the densities of the individual subbands, and the Hall slope gives the net free charge of the system n_{Hall}. For two spin-split electronlike subbands we expect $n_{\mathrm{Hall}} = n_1 + n_2$.

Figure 3(a) shows a zoom-in of Fig. 2(c) for the electron regime with the vertical axis scaled as $1/B_\perp$ to make the SdH oscillations periodic. A beating, visible as a π phase slip, is indicated with arrows. Figure 3(b) shows the power spectrum of the data in Fig. 3(a) for five gate voltage values. The frequency axis f has been multiplied by e/h to directly show the subband densities. At positive V_{TG}, the power spectrum reveals a single oscillation frequency. Decreasing V_{TG}, the peak moves to lower electron densities and gradually splits into two components. The amplitude of the low-density peak decreases with respect to its high-density counterpart (n_1) until it disappears in the background for $V_{TG} < -0.25$ V. The quench of the n_2 peak at finite density is compatible with a $k \neq 0$ minimum in the dispersion relation of the high energy split band, as just above energy II in Fig. 1(a).

Additional insight into the data is gained by comparing the peaks position with the Hall density. The same analysis as in Fig. 3(b) is shown in the color plot of Fig. 3(c) as a function of V_{TG}. The solid blue line indicates the density n_{Hall}, extracted from ρ_{xy}. The dashed line tracks the position of the n_1 peak in the power spectrum while the dotted line shows the quantity $n_{\mathrm{Hall}} - n_1$. For $V_{TG} > 0$, a single peak is visible in the spectrum with $fe/h = n_{\mathrm{Hall}}/2$. This is consistent with two spin degenerate bands with $n_1 = n_2$, as in scenario I in Fig. 1(a). Once the splitting develops, as highlighted in Fig. 3(c), $n_{\mathrm{Hall}} - n_1$ matches the position of the measured n_2 peak. The analysis is extended down to $V_{TG} = -0.46$ V, where ρ_{xy} does not show indication of hole transport yet. The density difference between the two subbands gradually increases until $n_{\mathrm{Hall}} = n_1$ at $V_{TG} \approx -0.4$ V; i.e., all mobile charge resides in a *single* band with $n_1 = 1.4 \times 10^{15}$ m^{-2}. This is compatible with situation II in Fig. 1(a).

Below the CNP, the electronlike n_1 peak coexists with a holelike state, highlighted with a dot-dashed line in Fig. 3(c). We confirmed that its position matches the periodicity of

the holelike LLs [cf. dots in Figs. 2(c) and 3(c)]. The hole signature in the spectrum can be interpreted as either two degenerate subbands $p_1 = p_2$ or one spin-orbit polarized subband p_1. Extracting the total density from the Hall slope is less accurate in this regime due to the nonlinearity of $\rho_{xy}(B)$, preventing further analysis. Nevertheless, assuming a single subband p_1, as predicted by our model for situation III in Fig. 1(b), the top gate capacitance in the hole regime $(-\partial p_1/\partial V_{\mathrm{TG}})$ matches that in the electron regime $(\partial n_{\mathrm{Hall}}/\partial V_{\mathrm{TG}})$, as expected from the electrostatic model of Fig. 1(a). Furthermore, the absence of Zeeman splitting in the holelike LL up to high field supports the interpretation that holes are also fully spin-orbit polarized. Assuming a single holelike band, the filling factors indicated in Fig. 3(c) with negative numbering are calculated for the holelike LLs, consistent with an identical filling factor for electron- and holelike LLs (1 and −1, respectively) being populated at the CNP [41,42]. From these observation we conclude that a single and fully spin-orbit polarized hole band p_1 is occupied below the CNP, consistent with scenario III in Fig. 1(b).

The intersection between p_1 and n_1 at $V_{\mathrm{TG}} \approx -0.6$ V determines the CNP, consistent with Fig. 2(b). The crossing of the Fermi energy with the top of the valence band is inferred to be at $V_{\mathrm{TG}} = -0.35$ V. This matches the peak in ρ_{xx}, as seen in Fig. 2(a), and the kink in n_{Hall} visible in Fig. 3(c) marking a change in gate capacitance as a screening layer is populated.

After demonstrating the large splitting at the CNP, we investigate how the large spin-orbit polarization affects transport phenomena. The zero field polarization of electronlike states, quantified as $(n_1 - n_2)/(n_1 + n_2)$, saturates at 100% for $V_{\mathrm{TG}} = -0.4$ V [Fig. 4(a)]. Despite expecting holelike states in this regime, hole conduction is not experimentally detected, by either a slope reversal in ρ_{xy} [Fig. 2(b)] or additional LLs in ρ_{xx} [Fig. 2(c)]. This behavior is presumably due to the low mobility of holes in GaSb which, for densities lower than 5×10^{14} m^{-2}, may localize. As only electronlike states contribute to transport, this situation effectively realizes a helical 2DEG. Such a system is reminiscent of the surface of three-dimensional topological insulators, where the Fermi energy crosses a single spin-resolved band, and might have potential interest for studying topological states of matter.

The full spin-orbit polarization for $V_{\mathrm{TG}} \approx -0.4$ V is further confirmed by the quantum Hall plateaus of ρ_{xy}^{-1}, shown in Fig. 4(b). At high electron density (orange line, $V_{\mathrm{TG}} = 0.25$ V) the plateaus evolve in steps of $2e^2/h$, as expected for a conventional 2DEG. For $B_\perp > 3$ T, Zeeman splitting lifts spin degeneracy, resulting in e^2/h plateaus. In the fully polarized regime (red line, $V_{\mathrm{TG}} = -0.4$ V), the plateaus exquisitely evolve as integer multiples of e^2/h from the first visible steps at $B_\perp \approx 400$ mT. This is further evidence of the helical nature of electronlike states, extending also to small magnetic fields. The oscillations

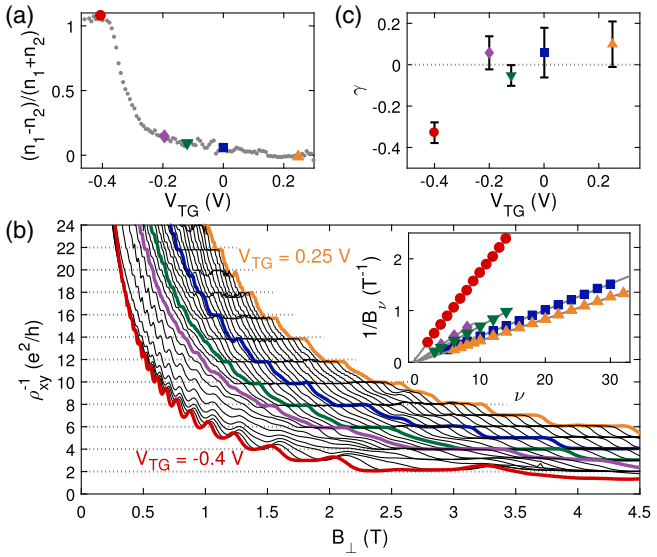

FIG. 4. (a) Spin-orbit polarization of electronlike states as a function of V_{TG}, with markers defined as in (b). (b) Inverse transverse resistivity ρ_{xy}^{-1} for different top gate voltages V_{TG}. Inset: Inverse magnetic field positions of the filling factors ν for different V_{TG} values. Solid lines are linear fits to the data. (c) Phase offset γ of the data in the inset of (b) extrapolated for $1/B \to 0$.

in the low-density plateaus [also visible in Fig. 2(b)] are attributed to disorder, resulting in a broadening of LLs and an eventual mixing between ρ_{xx} and ρ_{xy} [48]. We note that the overshoots in ρ_{xy}^{-1} or an eventual presence of holelike states do not compromise the analysis. In fact, the density of the system for $V_{\mathrm{TG}} = -0.4$ V is confirmed within 5% by three independent checks: (i) the slope of ρ_{xy}, constant up to $B_\perp = 5$ T; (ii) the periodicity of the low-field SdH oscillation; (iii) the magnetic field position B_ν of the $\nu e^2/h$ plateaus in ρ_{xy}^{-1}, satisfying $n_1 = \nu e B_\nu/h$.

The unique Fermi level crossing present in our system, together with strong SOC, can result in a nontrivial Berry phase acquired by electrons on a closed cyclotron orbit, such as in Fig. 1(c). To check this eventuality, we measured the phase offset φ of the SdH oscillations for $1/B \to 0$, similar to earlier work on graphene [49,50] and 3D topological insulators [51,52]. While conventional 2DEGs have $\varphi = 0$, materials with a symmetric Dirac cone exhibit $\varphi = 1/2$. In a complex band structure, as in the present case, the Berry phase is not expected to be quantized but to vary depending on the details of the dispersion relation [53]. The inset of Fig. 4(b) shows the $1/B_\nu$ positions of the ν filling factors for various top gate voltages (markers) together with linear fits (lines) extrapolating to $1/B \to 0$. The result of the extrapolation is shown in Fig. 4(c). For $V_{\mathrm{TG}} \geq -0.2$ V, all the curves consistently give $\varphi \approx 0$, as expected for normal fermions. For $V_{\mathrm{TG}} = -0.4$ V, the extrapolation leads a phase shift $\varphi = -0.33 \pm 0.05$, consistent with a nonzero Berry phase.

In conclusion, we studied the band structure of inverted InAs/GaSb QWs via magnetotransport measurements. Consistent with simulations, electronlike and holelike states are fully spin-orbit polarized in proximity of the CNP. We identify a regime where a single electronlike band with helical spin texture contributes to transport. The 100% spin-orbit polarization of the system is confirmed by quantum Hall plateaus evolving in e^2/h steps and a nontrivial Berry phase.

We thank Emmanuel Rashba, Joshua Folk, and Karsten Flensberg for valuable discussions. This work was supported by Microsoft Corporation Station Q. The work in Copenhagen was also supported by the Danish National Research Foundation and the Villum Foundation. The work in Delft was also supported by the Dutch Organisation for Scientific Research (NWO) and the Foundation for Fundamental Research on Matter (FOM). F. N. acknowledges support of the European Commission through the Marie Curie Fellowship, Grant Agreement No. 659653.

*fnichele@nbi.ku.dk

[1] M. J. Yang, C. H. Yang, B. R. Bennett, and B. V. Shanabrook, Phys. Rev. Lett. **78**, 4613 (1997).
[2] C. Liu, T. L. Hughes, X.-L. Qi, K. Wang, and S.-C. Zhang, Phys. Rev. Lett. **100**, 236601 (2008).
[3] F. Qu, A. J. A. Beukman, S. Nadj-Perge, M. Wimmer, B.-M. Nguyen, W. Yi, J. Thorp, M. Sokolich, A. A. Kiselev, M. J. Manfra, C. M. Marcus, and L. P. Kouwenhoven, Phys. Rev. Lett. **115**, 036803 (2015).
[4] F. Nichele, H. J. Suominen, M. Kjaergaard, C. M. Marcus, E. Sajadi, J. A. Folk, F. Qu, A. J. A. Beukman, F. K. de Vries, J. van Veen, S. Nadj-Perge, L. P. Kouwenhoven, B.-M. Nguyen, A. A. Kiselev, W. Yi, M. Sokolich, M. J. Manfra, E. M. Spanton, and K. A. Moler, New J. Phys. **18**, 083005 (2016).
[5] I. Knez, R.-R. Du, and G. Sullivan, Phys. Rev. Lett. **107**, 136603 (2011).
[6] K. Suzuki, Y. Harada, K. Onomitsu, and K. Muraki, Phys. Rev. B **87**, 235311 (2013).
[7] I. Knez, C. T. Rettner, S.-H. Yang, S. S. P. Parkin, L. Du, R.-R. Du, and G. Sullivan, Phys. Rev. Lett. **112**, 026602 (2014).
[8] L. Du, I. Knez, G. Sullivan, and R.-R. Du, Phys. Rev. Lett. **114**, 096802 (2015).
[9] S. Mueller, A. N. Pal, M. Karalic, T. Tschirky, C. Charpentier, W. Wegscheider, K. Ensslin, and T. Ihn, Phys. Rev. B **92**, 081303 (2015).
[10] Žutić Igor, J. Fabian, and S. Das Sarma, Rev. Mod. Phys. **76**, 323 (2004).
[11] We use the same subband definition as in Sec. 6.3.1 of Ref. [12].
[12] R. Winkler, *Spin-Orbit Coupling Effects in Two-Dimensional Electron and Hole Systems*, Springer Tracts in Modern Physics (Springer-Verlag, Berlin, 2003), Vol. 191.
[13] J. Luo, H. Munekata, F. F. Fang, and P. J. Stiles, Phys. Rev. B **38**, 10142 (1988).
[14] B. Das, D. C. Miller, S. Datta, R. Reifenberger, W. P. Hong, P. K. Bhattacharya, J. Singh, and M. Jaffe, Phys. Rev. B **39**, 1411 (1989).
[15] J. P. Heida, B. J. van Wees, J. J. Kuipers, T. M. Klapwijk, and G. Borghs, Phys. Rev. B **57**, 11911 (1998).
[16] S. Brosig, K. Ensslin, R. J. Warburton, C. Nguyen, B. Brar, M. Thomas, and H. Kroemer, Phys. Rev. B **60**, R13989 (1999).
[17] Y. S. Gui, C. R. Becker, N. Dai, J. Liu, Z. J. Qiu, E. G. Novik, M. Schäfer, X. Z. Shu, J. H. Chu, H. Buhmann, and L. W. Molenkamp, Phys. Rev. B **70**, 115328 (2004).
[18] M. Nishioka, B. A. Gurney, E. E. Marinero, and F. Mireles, Appl. Phys. Lett. **95**, 242108 (2009).
[19] H. L. Stormer, Z. Schlesinger, A. Chang, D. C. Tsui, A. C. Gossard, and W. Wiegmann, Phys. Rev. Lett. **51**, 126 (1983).
[20] B. Habib, E. Tutuc, S. Melinte, M. Shayegan, D. Wasserman, S. A. Lyon, and R. Winkler, Phys. Rev. B **69**, 113311 (2004).
[21] F. Nichele, A. N. Pal, R. Winkler, C. Gerl, W. Wegscheider, T. Ihn, and K. Ensslin, Phys. Rev. B **89**, 081306 (2014).
[22] G. M. Minkov, A. V. Germanenko, O. E. Rut, A. A. Sherstobitov, S. A. Dvoretski, and N. N. Mikhailov, Phys. Rev. B **89**, 165311 (2014).
[23] See Supplemental Material at http://link.aps.org/supplemental/10.1103/PhysRevLett.118.016801 for material and methods and a description of the numerical simulations, which includes Refs. [24–36].
[24] B.-M. Nguyen, W. Yi, R. Noah, J. Thorp, and M. Sokolich, Appl. Phys. Lett. **106**, 032107 (2015).
[25] J. Tukey, in *Proceedings of the Advanced Seminar on Spectral Analysis of Time Series* (Wiley, New York, 1967), pp. 25–46.
[26] F. Harris, Proc. IEEE **66**, 51 (1978).
[27] S. Luryi, Appl. Phys. Lett. **52**, 501 (1988).
[28] E. O. Kane, in *Handbook on Semiconductors*, edited by W. Paul (North-Holland, Amsterdam, 1982), Vol. 1, p. 193.
[29] G. Bastard, *Wave Mechanics Applied to Semiconductor Heterostructures* (Wiley, New York, 1988).
[30] M. G. Burt, J. Phys. Condens. Matter **4**, 6651 (1992).
[31] B. A. Foreman, Phys. Rev. B **56**, R12748 (1997).
[32] E. G. Novik, A. Pfeuffer-Jeschke, T. Jungwirth, V. Latussek, C. R. Becker, G. Landwehr, H. Buhmann, and L. W. Molenkamp, Phys. Rev. B **72**, 035321 (2005).
[33] A. J. Pfeuffer-Jeschke, Ph.D. thesis, Universität Würzburg, 2000.
[34] E. Halvorsen, Y. Galperin, and K. A. Chao, Phys. Rev. B **61**, 16743 (2000).
[35] P. Lawaetz, Phys. Rev. B **4**, 3460 (1971).
[36] T. Andlauer and P. Vogl, Phys. Rev. B **80**, 035304 (2009).
[37] A. Zakharova, S. T. Yen, and K. A. Chao, Phys. Rev. B **66**, 085312 (2002).
[38] J. Li, W. Yang, and K. Chang, Phys. Rev. B **80**, 035303 (2009).
[39] L.-H. Hu, C.-X. Liu, D.-H. Xu, F.-C. Zhang, and Y. Zhou, Phys. Rev. B **94**, 045317 (2016).

[40] I. Knez, R. R. Du, and G. Sullivan, Phys. Rev. B **81**, 201301 (2010).
[41] R. J. Nicholas, K. Takashina, M. Lakrimi, B. Kardynal, S. Khym, N. J. Mason, D. M. Symons, D. K. Maude, and J. C. Portal, Phys. Rev. Lett. **85**, 2364 (2000).
[42] F. Nichele, A. N. Pal, P. Pietsch, T. Ihn, K. Ensslin, C. Charpentier, and W. Wegscheider, Phys. Rev. Lett. **112**, 036802 (2014).
[43] S.-F. Tsay, J.-C. Chiang, Z. M. Chau, and I. Lo, Phys. Rev. B **56**, 13242 (1997).
[44] Y. Vasilyev, S. Suchalkin, K. von Klitzing, B. Meltser, S. Ivanov, and P. Kopev, Phys. Rev. B **60**, 10636 (1999).
[45] T. Ando, A. B. Fowler, and F. Stern, Rev. Mod. Phys. **54**, 437 (1982).
[46] P. T. Coleridge, R. Stoner, and R. Fletcher, Phys. Rev. B **39**, 1120 (1989).
[47] Y. A. Bychkov and E. I. Rashba, J. Phys. C **17**, 6039 (1984).
[48] B. Huckestein, Rev. Mod. Phys. **67**, 357 (1995).
[49] K. S. Novoselov, A. K. Geim, S. V. Morozov, D. Jiang, M. I. Katsnelson, I. V. Grigorieva, S. V. Dubonos, and A. A. Firsov, Nature (London) **438**, 197 (2005).
[50] Y. Zhang, Y.-W. Tan, H. L. Stormer, and P. Kim, Nature (London) **438**, 201 (2005).
[51] D.-X. Qu, Y. S. Hor, J. Xiong, R. J. Cava, and N. P. Ong, Science **329**, 821 (2010).
[52] J. Xiong, Y. Luo, Y. H. Khoo, S. Jia, R. J. Cava, and N. P. Ong, Phys. Rev. B **86**, 045314 (2012).
[53] A. R. Wright and R. H. McKenzie, Phys. Rev. B **87**, 085411 (2013).